Reactive astrocyte-driven epileptogenesis is induced by microglia initially activated following status epilepticus

Short title: Inter-glial communication underlies epileptogenesis after status epilepticus

Fumikazu Sano[1,2], Eiji Shigetomi[1], Youichi Shinozaki[1], Haruka Tsuzukiyama[1], Kozo Saito[1,3], Katsuhiko Mikoshiba[4], Kanji Sugita[2], Masao Aihara[2], Schuichi Koizumi[1]*

1 Department of Neuropharmacology, Interdisciplinary Graduate School of Medicine, University of Yamanashi, Yamanashi, Japan,

2 Department of Pediatrics, Faculty of Medicine, University of Yamanashi, Yamanashi, Japan,

3 Department of Neurology, Graduate School of Medical Science, Kyoto Prefectural University of Medicine, Kyoto, Japan,

4 Laboratory for Developmental Neurobiology, RIKEN Center for Brain Science, Saitama, Japan

19

20 *skoizumi@yamanashi.ac.jp (SK)

21

Abbreviations:

2-APB, 2-aminoethoxydiphenyl borate; CPA, cyclopiazonic acid; PBS, phosphate buffered saline; RT-PCR, reverse transcription-polymerase chain reaction; SE, status epilepticus; TTX, tetrodotoxin; WT, wild-type

Abstract

Extensive activation of glial cells during a latent period has been well documented in various animal models of epilepsy; however, it remains unknown whether such glial activation is capable of promoting epileptogenesis. Here, we show that temporally distinct activation profiles of microglia and astrocytes collaboratively contribute to epileptogenesis in a drug-induced status epilepticus model. We found that reactive microglia appear first, followed by reactive astrocytes and increased susceptibility to seizures. Pharmacological intervention against microglial activation reduces astrogliosis, aberrant astrocyte Ca^{2+} signaling, and seizure susceptibility. Reactive astrocytes exhibit larger Ca^{2+} signals mediated by IP_3R2, whereas deletion of this type of Ca^{2+} signaling reduces seizure susceptibility after status epilepticus. Together, our findings indicate that the sequential activation of glial cells constitutes a cause of epileptogenesis after status epilepticus.

Introduction

Epileptogenesis; i.e., the process leading to epilepsy, is a common sequel of brain insults such as brain injury, cerebrovascular disease, or status epilepticus (SE) [1,2] Such brain insults are typically followed by a latent period, during which the brain undergoes a cascade of morphological and functional changes over month to years prior to the onset of chronic epilepsy [3,4]. Extensive activation of glial cells, including microglia and astrocytes, has been well documented during this latent period in various animal models of epilepsy [5–7]. Although the association of pathology with reactive glial cells is widely recognized, it is unclear whether such microglial and astrocytic activation constitutes primary causes of epilepsy or rather represents the results of repeated seizures. Moreover, the potential for these reactive glial cells to comprise candidates for epileptogenesis raises the further mechanistic question regarding whether activated glial cells might contribute to epileptogenesis independently or collaboratively.

In chemoconvulsant-induced epilepsy models, microglia are activated and produce pro-inflammatory mediators immediately following seizure onset [8]. Activated microglia can decrease the seizure threshold in animal models by

61 releasing pro-inflammatory molecules with neuromodulatory properties [9].
62 Notably, the extent of microglial activation correlates with the seizure frequency
63 in human drug-resistant epilepsy [10]. Alternatively, such microglial activation
64 may not persist chronically. For example, pro-inflammatory molecules are
65 detectable in microglia following a seizure but the expression diminishes after
66 several hours [11]. Furthermore, although the activation of microglia is well
67 characterized, it is unclear whether these activated microglia affect developing
68 epileptogenic processes directly or through the modulation of other cells, such
69 as subsequent astrocytic activation.

70 Reactive astrogliosis is also one of the most common pathological features in
71 epilepsy and other brain insults [12,13]. Although reactive astrogliosis is
72 considered the consequence of repetitive seizures, some evidence that reactive
73 astrocytes may be responsible for repetitive seizures is available. In the epileptic
74 brain, reactive astrocytes exhibit physiological and molecular changes, such as
75 reduced inward rectifying K^+ current [14], changes in transporters [15], or
76 release of gliotransmitters [16] that may underlie neuronal hyperexcitability [17].
77 Although astrocytes do not exhibit prominent electrical excitability as observed in
78 neurons, they are able to dynamically regulate calcium using internal stores

79 [18,19]. Calcium transients in astrocytes are thought to modulate the release of a
80 number of gliotransmitters that could influence synaptic function, synapse
81 formation [20–22], and neural circuit excitability [23]. In particular, several
82 previous studies showed that astrocyte calcium activity could contribute to
83 excitotoxic neuronal death through glutamate release following SE [24,25].
84 However, the functional changes including Ca^{2+} signaling of reactive astrocytes
85 after SE and their causal roles in epileptogenesis remain largely uncertain.
86 To evaluate the role of inter-glial communication between different types of
87 glial cells in the process of epileptogenesis, we assessed the spatiotemporal
88 dynamics of glial activation following SE. Using cell-type specific manipulation,
89 we show that relative alterations of both microglia and astrocytes play causal
90 roles in epileptogenesis. Moreover, reactive glia are temporally distinct and
91 collaboratively contribute to epileptogenesis. Reactive microglia appear first and
92 induce reactive astrocytes in the hippocampus after SE. These reactive
93 astrocytes present larger IP_3R2-mediated Ca^{2+} signals, which are essential for
94 induction of the increased seizure susceptibility after SE. We clearly
95 demonstrate that inhibition of microglial activation reduces astrogliosis, aberrant
96 astrocytic Ca^{2+} signaling, and seizure susceptibility. We therefore conclude that

the sequential activation of glial cells; i.e., the initial activation of microglia followed by astrocytic activation, is a cause of epileptogenesis after SE.

Results

Astrocytic activation follows microglial activation after SE

To determine the contributions of glial cells to epileptogenesis, we used the pilocarpine model of epilepsy in mice, a model known to be highly isomorphic with human temporal lobe epilepsy [26,27]. Repeated low doses of pilocarpine (100 mg kg^{-1}) were injected intraperitoneally (i.p.) until the onset of SE (Fig 1A). This ramping protocol has been shown to reduce mortality after SE [28,29]. To investigate how glial cell activation affects the epileptogenic process, we first examined the spatiotemporal pattern of microglial and astrocytic activation in the hippocampus following SE. We initially assessed microglial and astrocytic activation with immunohistochemistry using cell-type-specific activation markers at 1, 3, 7, and 28 days after SE (Fig 1B and 1D). The area of Iba1-positive microglia was significantly increased in CA1 from 1 to 7 days after SE, which was followed by an increase in the area of GFAP-positive astrocytes in CA1 from

115 7 to 28 days after SE (Fig 1C and 1E).

116

117 **Fig 1. Astrogliosis is observed following microglial activation after SE.**

118 (A) As shown in the experimental protocols, mice were administered pilocarpine
119 to achieve stage 5 seizures. The second SE was induced using the same
120 protocol 4 weeks after the first SE. SP (PP) indicates that mice were injected
121 with saline (pilocarpine) at 8 weeks of age followed by an injection of pilocarpine
122 at 12 weeks of age. (B and C) Representative microphotographs showing the
123 spatiotemporal characteristics of Iba-1 (B) or GFAP (C) expression in CA1 after
124 SE. Fifteen images were captured per z-stack image (0.5 μm step). Cont,
125 control; D, day. (D and E) Quantification of the temporal profile of Iba-1 positive
126 microglia (D) or GFAP positive astrocytes (E) after SE (n = 5 mice (D); n = 5, 5,
127 5, 5, 7 mice, (E), *P < 0.05, **P < 0.01 vs. control, one-way ANOVA (P < 0.001)
128 with Dunnett's test). (F) Dot plots showing dose of pilocarpine required for the
129 induction of the second SE (n = 14, 13 mice, *P < 0.05, Mann–Whitney U-test).
130 (G) Scatter plot showing dose of pilocarpine required for the induction of the first
131 (at 8 weeks of age) and second (at 12 weeks of age) SE in the PP group (n = 13
132 mice, **P < 0.01, Wilcoxon signed-rank test). Values represent the means ±

SEM.

To examine whether the first SE increased seizure susceptibility, the second SE was induced 4 weeks after the first SE. A lower dose of pilocarpine was required for the induction of the second SE in mice with prior exposure to pilocarpine-induced SE at 8 weeks of age (PP) compared to those without such exposure (SP) (Fig 1F). In addition, a lower dose of pilocarpine was required for the induction of the second SE compared to the first SE (Fig 1G). These data indicated that the first SE increased seizure susceptibility at 4 weeks after the first SE. A comparison with the results in Fig 1 suggested that the temporal pattern of astrocyte activation, rather than that of microglia, correlates well with the increase of seizure susceptibility.

Ca^{2+} hyperactivity via IP_3R2 in reactive astrocytes after SE

To examine the SE-induced functional changes in astrocytes, Ca^{2+} imaging was performed from hippocampal slices prepared from wild-type (WT) and Glast-CreERT2::flx-GCaMP3 mice [30,31]. Astrocytes displayed significantly larger and more frequent Ca^{2+} signals approximately 4 weeks after SE (S1

151 Movie). To test whether hyperactivity of astrocytes is influenced by neuronal
152 hyperactivity, we blocked neuronal transmission by topically applying the
153 voltage-gated sodium channel blocker tetrodotoxin (TTX; 1 μM). TTX did not
154 affect the amplitude of astrocytic Ca^{2+} signals (Fig 2A, 2D and 2E) (S2 Movie).
155
156 **Fig 2. Reactive astrocytes exhibit IP_3R2-mediated Ca^{2+} hyperactivity, which**
157 **is essential for epileptogenesis.**
158 (A-C) Ca^{2+} dynamics of astrocytes approximately 4 weeks after SE in the CA1
159 stratum radiatum region in Glast-CreERT2::flx-GCaMP3 mice before and after
160 TTX (1 μM) (A), CPA (20 μM) (B), and 2-APB (100 μM) (C) application. (D-I) Box
161 plots showing amplitudes of Ca^{2+} signals before and after TTX (1 μM) (D), CPA
162 (20 μM) (F), and 2-APB (100 μM) (H) application. (n = 10, 13, 14 cells/2 mice,
163 ***$P < 0.001$, unpaired t-test). Cont, control. Cumulative probability plots
164 showing amplitudes (dF/F) of Ca^{2+} signals before and after TTX (not significant
165 ($P > 0.05$), Kolmogorov–Smirnov test) (E), CPA ($P < 0.001$, Kolmogorov–
166 Smirnov test) (G), and 2-APB ($P < 0.001$, Kolmogorov–Smirnov test) (**I**)
167 application. (J) Astrocytic Ca^{2+} dynamics by Fluo4 in the CA1 stratum radiatum
168 region in WT control, WT after SE, and IP_3R2KO mice after SE. (K-N) Box plots

showing Ca^{2+} signal amplitudes (dF/F) (K) and frequency (M) (n = 57, 32, 85 cells/2, 2, 3 mice, ***P < 0.001, unpaired t-test). Cumulative probability plots showing Ca^{2+} signal amplitudes (dF/F) (L) and frequency (N) (P < 0.001, Kolmogorov–Smirnov test). (O) Dot plots showing dose of pilocarpine required for the induction of the second SE in IP_3R2KO mice. SP (PP) indicates mice were injected with saline (pilocarpine) at 8 weeks of age followed by an injection of pilocarpine at 12 weeks of age. (n = 10 mice, N.S., not significant (P > 0.05), Mann–Whitney U-test). (P) Scatter plot showing dose of pilocarpine required for the induction of the first (at 8 weeks of age) and second (at 12 weeks of age) SE in the PP group regarding IP3R2KO mice (n = 10 mice, N.S., not significant (P > 0.05), Wilcoxon signed-rank test). Note: The first pilocarpine did not affect the dose required for the second SE in IP_3R2KO, see Fig 1G.

To elucidate the molecular mechanisms involved in astrocytic Ca^{2+} hyperactivity, we applied cyclopiazonic acid (CPA; 20 μM) to deplete intracellular calcium stores. CPA significantly reduced the amplitude of astrocytic Ca^{2+} signals after SE (Fig 2B, 2F and G) (S2 Movie). Then, we applied the membrane-permeable IP_3 receptor antagonist 2-aminoethoxydiphenyl borate

(2-APB; 100 μM). 2-APB also significantly reduced the amplitude of astrocytic Ca^{2+} signals after SE (Fig 2C, 2H and 2I) (S4 Movie). To confirm that astrocytic Ca^{2+} hyperactivity is completely dependent on the IP_3 receptor, we performed Ca^{2+} imaging in IP_3R2 knockout (KO) mice [32]. The amplitude of astrocytic Ca^{2+} signals after SE was significantly decreased in IP_3R2KO mice compared with that in WT (Fig 2J, 2K, 2L, 2M and 2N). The frequency of astrocytic Ca^{2+} signals after SE was also significantly decreased in IP_3R2KO mice (Fig 2M and 2N) (S5 Movie). These results suggested that astrocytic Ca^{2+} hyperactivity after SE should be dependent on IP_3R2-mediated Ca^{2+} release from internal stores.

IP_3R2KO mice exhibit rescue of the increased seizure susceptibility

To clarify the role of astrocytic Ca^{2+} hyperactivity after SE in epileptogenesis, we investigated seizure susceptibility after SE in IP_3R2KO mice [32]. No differences in the dose of pilocarpine required for the induction of the first SE were observed between IP_3R2KO and WT mice (Fig 1F and 2O). These data indicated that IP_3R2-mediated Ca^{2+} signaling in astrocytes does not alter the acute responses to pilocarpine.

In IP_3R2KO mice, the area of Iba1-positive microglia was significantly

increased in CA1 at 1 day after SE, suggesting that microglial activation after SE was comparable in IP_3R2KO and WT mice (S1 Fig). However, there was no significant change in the dose of pilocarpine required for the induction of the second SE in SP compared with PP mice (Fig 2O). There was no significant change in the dose of pilocarpine required for the induction of the first and second SE in IP_3R2KO mice (Fig 2P). These results suggested that IP_3R2-mediated astrocytic Ca^{2+} hyperactivity is essential for the induction of the increased seizure susceptibility after SE.

Microglia inhibition reduces activated astrocyte morphology

Our data indicated temporal differences between activation of microglia and astrocytes; i.e., earlier and later onset after SE, respectively. To reveal features of the activated microglia after SE, we investigated the changes in mRNA levels of pro-inflammatory cytokines that are relevant to microglial activation by quantitative reverse transcription-polymerase chain reaction (RT-PCR) (Fig 3A, 3B and 3C). SE increased *Tnf* and *Il1b* mRNA in the hippocampus at 1 day after SE (Fig 3B and 3C). To explore the microglia-triggered astrocyte activation, we investigated microglial functional changes after SE. Among several molecules

tested, we found that *Tnf* and *Il1b* mRNAs were also significantly upregulated in the isolated hippocampal microglia at 1 day after SE (Fig 3A).

Fig 3. Microglia inhibition with minocycline and depletion with CSF1R antagonist (PLX5622) reduces astrogliosis.

(A) Microfluidic quantitative RT-PCR analysis of mRNA in total RNA extracted from hippocampal microglia after SE. Relative ratios of *Gapdh*-normalized mRNA to the corresponding control (Cont) are shown (n = 3 samples/9 mice, ***$P < 0.001$ vs. control, one-way ANOVA ($P < 0.01$, $P < 0.001$) with Dunnett's test). (B and C) Quantitative RT-PCR analysis of *Tnf* and *Il1b* mRNA in total hippocampal RNA after SE. Relative ratios of *Gapdh*-normalized mRNA to the corresponding control are shown (n = 5 mice, *$P < 0.05$, ***$P < 0.001$ vs. control, one-way ANOVA ($P < 0.001$, $P < 0.05$) with Dunnett's test). (D) Experimental scheme for minocycline post-treatment-mediated microglia inhibition. (E-H) Representative microphotographs showing the spatiotemporal characteristics of Iba-1 (E) and GFAP (F) expression and quantification of Iba-1 positive microglia (G) and GFAP positive astrocytes (H) in CA1 with or without minocycline post-treatment after SE. Fifteen images were collected per z-stack image (0.5

241 μm step). (n = 5 mice, N.S., not significant ($P > 0.05$), *$P < 0.05$, ***$P < 0.001$,
242 one-way ANOVA ($P < 0.01$) with Bonferroni test). (I and J) Quantitative RT-PCR
243 analysis as in (B and C) with or without minocycline post-treatment. (n = 5 mice,
244 N.S., not significant ($P > 0.05$), *$P < 0.05$, unpaired t-test). (K) Experimental
245 scheme for PLX5622-mediated microglia depletion. (L-O) Representative
246 microphotographs showing the spatiotemporal characteristics of Iba-1 (L) and
247 GFAP (M) expression and quantification of Iba-1 positive microglia (N) and
248 GFAP positive astrocytes (O) in CA1 with or without PLX5622 after SE. Fifteen
249 images were captured per z-stack image (0.5 μm step). (n = 5 mice, *$P < 0.05$,
250 **$P < 0.01$ vs. control of AIN-76A (control diet), ##$P < 0.01$ vs. control of
251 PLX5622, §$P < 0.05$, §§$P < 0.01$, §§§$P < 0.001$ vs. AIN-76A (corresponding day),
252 one-way ANOVA ($P < 0.01$) with Dunnett's test and unpaired t-test). (P)
253 Quantitative RT-PCR analysis as in (B and C) with or without PLX5622. (n = 5
254 mice, *$P < 0.05$, **$P < 0.01$, unpaired t-test).
255
256 To clarify whether microglial activation is required for astrogliosis, we
257 investigated the effect of post-treatment with the inhibitor, minocycline (Fig 3D)
258 [33–35]. To confirm the efficacy of minocycline in this protocol, microglial

activation was assessed by immunohistochemistry and quantitative RT-PCR. Minocycline post-treatment prevented the increase in the area of Iba1-positive cells in CA1 at 3 days after the first SE (Fig 3E and 3G) along with an increase in *Tnf* but not *Il1b* mRNA in the hippocampus at 1 day after the first SE (Fig 3I and 3J). Notably, microglia inhibition with minocycline post-treatment prevented the increase in the area of GFAP-positive cells in CA1 at 28 days after the first SE (Fig 3F and 3H).

To further confirm that acute microglial activation plays an important role in the morphological activation of astrocytes after SE, we applied PLX5622, a CSF1R antagonist, to deplete microglia (Fig 3K) [36–38]. PLX5622 treatment prevented the increase in the area of Iba1-positive cells in CA1 from 1 to 7 days after the first SE (Fig 3L and 3N). In addition, *Aif1* and *Tnf* mRNA levels were significantly decreased at 1 day after SE with PLX5622 treatment compared with those in the control diet group (Fig 3P). Similarly, the increased area of GFAP-positive astrocytes in CA1 from 7 to 28 days after SE in control diet (AIN-76A) mice was prevented in PLX5622 treated mice (Fig 3M and 3O). To identify the optimal timing of microglial inhibition to prevent astrogliosis, we applied PLX5622 from 3 weeks after SE (Fig 4A). This later PLX5622 treatment

277 decreased the area of Iba1-positive cells in CA1 at 28 days after the first SE (Fig
278 4B and 4D) but did not prevent the increased area of GFAP-positive astrocytes
279 (Fig 4C and 4E). These findings showed that the initial reactive microglia are
280 required to induce morphological activation of astrocytes after SE.
281
282 **Fig 4. Microglia depletion with CSF1R antagonist (PLX5622) at late phase**
283 **after SE does not reduce astrogliosis and increased seizure susceptibility.**
284 (A) Experimental scheme for microglia depletion with PLX5622 at the late phase
285 after SE. (B and C) Representative microphotographs showing the
286 spatiotemporal feature of Iba-1 (B) and GFAP (C) expression in CA1 with or
287 without PLX5622 after SE. Fifteen images were collected per z-stack image (0.5
288 μm step). Cont, control; D, day. (D and E) Quantification of the temporal profile
289 of Iba-1 positive microglia (D) and GFAP positive astrocytes (E) after SE (n = 5
290 mice, ***P < 0.01 vs. control, unpaired t-test, ###P < 0.01 vs. AIN-76A
291 (corresponding day), one-way ANOVA (P < 0.001) with Dunnett's test). Values
292 represent the means ± SEM.
293
294 **Microglia inhibition reduces astrocytic Ca^{2+} hyperactivity**

We then investigated whether microglial activation is required for astrocytic Ca^{2+} hyperactivity after SE. We also used a pharmacological approach to inhibit the early microglial activation after SE. Microglia inhibition with minocycline reduced the larger and frequent Ca^{2+} signals of astrocytes (S1 Movie) (Fig 5A, 5B, 5C, 5D and 5E). Similarly, the amplitude and frequency of fluo-4AM-labeled astrocytic Ca^{2+} signaling after SE were significantly increased in control diet (AIN-76A) mice (Fig 5F, 5H, 5I, 5J and 5K) (S6 Movie). Conversely, the larger and frequent Ca^{2+} signals after SE were significantly reduced by the PLX5622 treatment (Fig 5G, 5L, 5M, 5N and 5O) (S7 Movie). These results indicated that acute microglial activation is essential for the changes of astrocytic Ca^{2+} activity after SE.

Fig 5. Microglia inhibition with minocycline or CSF1R antagonist (PLX5622) reduces the increased astrocytic Ca^{2+} hyperactivity following SE.

(A) Ca^{2+} dynamics of astrocytes approximately 4 weeks after SE in the CA1 stratum radiatum region in Glast-CreERT2::flx-GCaMP3 mice with or without minocycline treatment. (B-E) Box plots showing Ca^{2+} signal amplitude (dF/F) (B) and frequency (D) (n = 74, 92, 93 cells/3 mice, N.S., not significant ($P > 0.05$),

313 ***P < 0.001, unpaired t-test). Cumulative probability plots showing Ca^{2+} signal
314 amplitude (dF/F) (P < 0.001, Kolmogorov–Smirnov test) (C) and frequency (not
315 significant (P > 0.05), Kolmogorov–Smirnov test) (E). (F and G) Ca^{2+} dynamics
316 of astrocytes approximately 4 weeks after SE in the CA1 stratum radiatum
317 region in Glast-CreERT2::flx-GCaMP3 mice with (G) or without (F) PLX5622
318 treatment. (H-K) Box plots showing Ca^{2+} signal amplitude (dF/F) (H) and
319 frequency (J) in the AIN-76A (control diet) group. (n = 70, 58 cells/2 mice, ***P <
320 0.001, unpaired t-test). Cumulative probability plots showing Ca^{2+} signal
321 amplitude (dF/F) (P < 0.001, Kolmogorov–Smirnov test) (I) and frequency (P <
322 0.001, Kolmogorov–Smirnov test) (K) in the AIN-76A (control diet) group. (L-O)
323 Box plots showing Ca^{2+} signal amplitude (dF/F) (L) and frequency (M) in the
324 PLX5622 group. (n = 61, 71 cells/2 mice, N.S., not significant (P > 0.05),
325 unpaired t-test). Cumulative probability plots showing Ca^{2+} signal amplitude
326 (dF/F) (not significant (P > 0.05), Kolmogorov–Smirnov test) (M) and frequency
327 (not significant (P > 0.05), Kolmogorov–Smirnov test) (O) in the PLX5622 group.
328
329 **Microglia inhibition rescues enhanced seizure susceptibility**
330 Finally, we tested whether microglia inhibition rescued the increased seizure

susceptibility following SE. Post-treatment with minocycline following the first SE prevented the increased seizure susceptibility (Fig 6A and 6B). No difference was observed between control diet and PLX5622-treated mice in the dose of pilocarpine required for the induction of the first SE (Fig 6C), indicating that microglia inhibition does not alter the acute responses to pilocarpine. In contrast, a lower dose of pilocarpine was required for the induction of the second SE in control mice compared with that in PLX5622-treated mice (Fig 6D). Consistent with this, unlike the enhanced seizure susceptibility observed in control mice following the first SE (as indicated by the reduced dose of pilocarpine required to induce the second vs. the first SE), there was no significant change in the dose of pilocarpine required for the induction of the first or second SE in PLX5622-treated mice (Fig 6E and 6F). In contrast, a lower dose of pilocarpine was required for the induction of the second SE in later PLX5622 treatment mice, similar to that in control diet mice (Fig 6G, 6H, 6I and 6J). These data suggested that the inhibition of initial microglial activation rescues the increased seizure susceptibility.

Fig 6. Microglia inhibition with minocycline or CSF1R antagonist (PLX5622)

reduces the increased seizure susceptibility following SE.

(A) Dot plots showing dose of pilocarpine required for the induction of the second SE (n = 10 mice, N.S., not significant ($P > 0.05$), *$P < 0.05$, Mann–Whitney U-test). SMP (PMP) indicates that mice were injected with saline (pilocarpine) at 8 weeks of age with minocycline post-treatment followed by an injection of pilocarpine at 12 weeks of age. (B) Scatter plot showing dose of pilocarpine required for the induction of the first (at 8 weeks of age) and second (at 12 weeks of age) SE. (n = 10 mice, **$P < 0.01$, Wilcoxon signed-rank test). (C and D) Dot plots showing dose of pilocarpine required for the induction of the first (C) and second (D) SE with or without PLX5622. (n = 10, 8 mice, N.S., not significant ($P > 0.05$), **$P < 0.01$, Mann–Whitney U-test). AIN, control diet (AIN-76A). (E and F) Scatter plot showing dose of pilocarpine required for the induction of the first (at 8 weeks of age) and second (at 12 weeks of age) SE for AIN-76A (control diet) (E) or PLX5622 (F). (n = 10, 8 mice, N.S., not significant ($P > 0.05$), **$P < 0.01$, Wilcoxon signed-rank test). (G and H) Dot plots showing dose of pilocarpine required for the induction of the first (G) and second (H) SE with or without late PLX5622 treatment. (n = 10 mice, N.S., not significant ($P > 0.05$), Mann–Whitney U-test). (I and J) Scatter plot showing dose of pilocarpine

367 required for the induction of the first (at 8 weeks of age) and second (at 12
368 weeks of age) SE AIN-76A (control diet) (I) or PLX5622 (J). (n = 10 mice, **P <
369 0.01, Wilcoxon signed-rank test).
370
371 **Discussion**
372 Here, we demonstrate that SE induces sequential activation of glial cells; i.e., the
373 initial activation of microglia, followed by astrocytic activation, which is essential
374 for seizure susceptibility or epileptogenesis. The main findings in the present
375 study are as follows. (1) Microglia are activated and pro-inflammatory cytokines
376 of microglia are increased immediately after SE. (2) Reactive astrocytes, which
377 exhibit larger IP_3R2-mediated Ca^{2+} signals, appear following microglial activation
378 after SE. (3) Genetic deletion of IP_3R2 rescues both the aberrant Ca^{2+} signals in
379 astrocytes and the increased seizure susceptibility. (4) Pharmacological
380 inhibition of microglial activation or deletion of microglia reduces astrogliosis
381 along with aberrant Ca^{2+} signals of astrocytes, and rescues the increased
382 seizure susceptibility. These findings indicate that initially activated microglia are
383 responsible for the subsequent induction of epileptogenic reactive astrocytes in
384 vivo.

Microglial and astrocytic activation is a common feature of various central nervous system (CNS) disorders including epilepsy [39–42]. However, the pathological significance and spatiotemporal pattern of microglial and astrocytic activation in the epileptogenic process have not been carefully addressed. Microglial response to SE occurs immediately, with reactive microglia playing both detrimental and beneficial roles during acute seizures [43]. Although activated microglia exhibit a neuroprotective role via the P2Y12 receptor in the acute phase, they exert proconvulsive effects through the production of pro-inflammatory cytokines such as IL-1β [11], TNF [44], and IL-6 [45,46]. However, such increase of purinergic receptors and pro-inflammatory cytokines after SE may be transient [11], and it is unknown how this transient microglial activation including pro-inflammatory cytokines causes long-term epileptic potential. Here, we found that inhibiting microglia at the acute phase (0 to 7 days after SE) but not the late phase (21 to 28 days after SE) reduced susceptibility to the second SE, suggesting that activated microglia trigger the epileptogenic process including astrocytic activation, but do not exert a direct proconvulsive effect on the later phase after SE.

In the present study, we demonstrate that astrocytic activation develops

403 slowly starting 7 days after SE, is long lasting, and still observed when mice
404 show increased seizure susceptibility. Astrogliosis is thought to contribute to the
405 pathophysiology of epilepsy [47–49]. However, the role of astrogliosis in
406 epileptogenesis is largely unknown. In particular, it is important to determine
407 whether activated astrocytes play a proconvulsive or anticonvulsive role in the
408 epileptic brain. It has been proposed that astrocytic Ca^{2+} signaling contributes to
409 the induction of epileptic seizures and neuronal cell loss by seizures
410 [27,28,50,51]. In this study, we observed larger Ca^{2+} signals in the somatic
411 regions of astrocytes in the latent phase of epileptogenesis. Analysis of the Ca^{2+}
412 signals in astrocytes suggests that these Ca^{2+} signals are mediated by IP_3R2.
413 Notably, we found that genetic deletion of IP_3R2 is sufficient to rescue the
414 increased seizure susceptibility and reduce astrogliosis. Our study thus
415 suggests that IP_3R2-mediated Ca^{2+} signaling in reactive astrocytes plays a
416 proconvulsive role in the epileptic brain and can contribute to epileptogenesis.
417 Astrocytic Ca^{2+} signals may contribute to epileptogenesis through several
418 mechanisms. Astrocytes impact neural circuit excitability directly by releasing
419 “gliotransmitters”, such as glutamate [23,52,53]. Astrocytes also increase
420 neuronal excitability by forming new circuits through the release of synaptogenic

421 molecules [22,54]. However, the functional consequences of these changes in
422 the context of epileptogenesis remain to be determined. As Ca^{2+} serves as a
423 ubiquitous intracellular signal in the regulation of numerous cellular processes
424 including exocytosis, proliferation, and gene expression, it is also likely to
425 regulate many processes in the induction/maintenance of reactive astrocytes
426 [55,56]. Although it is difficult to exclude the inherent influence on the neural
427 circuit resulting from the deletion of IP_3R2, we demonstrate that SE induces
428 neither an increase in Ca^{2+} excitation in astrocytes nor proconvulsive effects in
429 IP_3R2KO mice, suggesting that enhanced Ca^{2+} signals in astrocytes are likely
430 responsible for epileptogenesis.

431 In animal models of epilepsy, reactive astrocytes undergo extensive
432 physiological changes involving not only Ca^{2+} signaling but also ion and
433 neurotransmitter homeostasis along with intracellular and extracellular water
434 content, which can cause neuronal hyperexcitability [57–60]. The relative
435 importance of such functional changes of astrocytes to epileptogenesis will be
436 investigated in future studies. Recently, it has been reported that activated
437 microglia can induce neurotoxic reactive astrocytes (i.e., A1 astrocytes), which
438 release unidentified neurotoxic factors [37,61]. Thus, whether astrogliosis after

SE results in a similar phenotype to A1 astrocytes and whether IP_3-mediated Ca^{2+} signals contribute to the induction of neurotoxic phenotype [56] represent relevant issues to be addressed in future investigations. Although whether the astrocytes induced by activated microglia are in a primarily neurotoxic or neuroprotective state remains largely unknown, our data suggest that the reactive astrocytes induced by activated microglia after SE exert proconvulsive effects in the epileptic brain.

In this study, we also demonstrate that pro-inflammatory cytokines of microglia are increased prior to astrocytic activation, suggesting the importance of microglial activation as an initial process of epileptogenesis. Pharmacological inhibition and depletion of microglia significantly blocked the activation of astrocytes and decreased the seizure threshold after SE. Our findings identify that activated microglia likely promote epileptogenesis by inducing the proconvulsive phenotype of astrocytes. Although it has been recognized that microglial activation occurs before reactive astrogliosis in various CNS diseases [62—64], little was known prior to the present study regarding how microglial-astrocytic interactions contribute to the pathophysiology of epilepsy. For example, several previous studies using chemoconvulsant-induced epilepsy

models have shown that activated microglia were present immediately after SE and that functional changes occurred, such as upregulation of pro-inflammatory cytokines [8,65,66], purinergic receptors [39], and phagocytosis [40].

Previous reports also revealed that microglia modulate astrocyte activation via various molecules, especially pro-inflammatory cytokines [67,68]. Consistent with this, we found that TNF and IL-1β are significantly upregulated in hippocampal microglia at 1 day after SE. Conversely, microglia inhibition by minocycline prevents the increased mRNA of TNF in the hippocampus at 1 day after the first SE along with subsequent reactive astrogliosis, suggesting a potential role of pro-inflammatory cytokines from microglia in reactive astrogliosis after SE. As the effect of minocycline may not be restricted to microglia, we depleted microglia using a CSF-1 receptor antagonist and found similar results, suggesting that microglial activation occurs through cytokine release. Thus, despite the potential problem of specificity owing to the use of pharmacological inhibition of microglia, we clearly show that initial activation of microglia and microglia-derived proinflammatory cytokines likely underlie the subsequent astrogliosis-mediated epileptogenesis. Nevertheless, because the molecular mechanisms underlying the activation of astrocytes triggered by

activated microglia have not been fully clarified, other chemical mediators such as ATP may also contribute to activate microglia-mediated astrogliosis [69]. Further investigations using more specific interventions are required to elucidate the precise molecular mechanisms underlying the interaction between microglia and astrocytes.

In summary, our findings identify a sequence of glial activation in the hippocampus that contributes to the epileptogenic process. In this process, microglial activation is identified as a crucial event to induce reactive astrocytes. In turn, astrocytic Ca^{2+} activation mediated by IP_3R2 was essential for the induction of epileptogenesis. Our findings add to the emerging view that reactive astrocytes triggered by microglia have a central role in the pathogenesis of epilepsy and, given the limited progress of neuron-centered epilepsy research over the past several years, suggest reactive astrocytes as promising new targets for the development of alternative and more specific antiepileptic drugs.

Materials and Methods

Animals

All studies used male C57BL/6J mice (SLC Japan, Shizuoka, Japan). IP_3R2KO mice on a C57BL/6 background were available from a previous study [32]; their generation and maintenance have been previously described in detail. Glast-CreERT2::flx-GCaMP3 mice on a C57BL/6 background were also available from a previous study [30,31]; their generation and maintenance have been previously described in detail. In the present study, we performed immunohistochemistry and confirmed that GCaMP3 was co-localized with GFAP, an astrocyte marker, but not with Iba1 or NeuN (S2 Fig and S1 Table). Overall, Ca^{2+} signals detected by GCaMP3 were mainly detected from astrocytes.

Mice were housed on a 12 h light (6 am)/dark (6 pm) cycle with ad libitum access to water and rodent chow. The animals were allowed to adapt to laboratory conditions for at least 1 week before starting the experiments. All experimental procedures were performed in accordance with the “Guiding Principles in the Care and Use of Animals in the Field of Physiologic Sciences” published by the Physiologic Society of Japan and with the previous approval of

509 the Animal Care Committee of Yamanashi University (Chuo, Yamanashi,
510 Japan).
511
512 **Animal treatments**
513 The first SE was induced in 8-week-old male mice by the administration of
514 pilocarpine and the second SE was induced 4 weeks after the first SE. A low
515 dose of 100 mg kg^{-1} pilocarpine (Wako, 161-07201) per injection was
516 administered i.p. every 20 min until the onset of Racine scale stage 5 seizures.
517 Scoporamin methyl bromide (1 mg kg^{-1}, i.p., Wako, 198-07971) was
518 administered 30 min prior to pilocarpine injection to reduce its peripheral effects
519 [28,29]. Seizures were terminated with pentobarbital (20 mg kg^{-1}, i.p., Kyoritu
520 Seiyaku) when mice experienced stage 5 seizures for 30 min. Behavior of
521 pilocarpine-treated mice was observed for 1 h after SE.
522 To establish whether minocycline inhibits acute seizure-induced microglial
523 activation, mice were administered i.p. with saline or minocycline (25 mg kg^{-1}) 1
524 h after pilocarpine-SE induction and for the following two consecutive days [33–
525 35]. Microglia were also depleted from mice by treatment with the CSF1R
526 antagonist, PLX5622 (Plexxikon), formulated in AIN-76A rodent chow (Research

Diets). Mice were treated with PLX5622 (1200 mg kg^{-1} Chow) or a matched control diet (AIN-76A) for seven days before SE and for the following seven consecutive days [36–38].

Immunohistochemistry

The mice were deeply anesthetized with pentobarbital and perfused transcardially with phosphate buffered saline (PBS), followed by 4% (w/v) paraformaldehyde in PBS. The brains were removed, postfixed overnight, then cryoprotected with 30% (w/v) sucrose in PBS for two days. The brains were frozen and coronal sections (20 μm) were cut using a cryostat (Leica CM1100). Slices were washed with PBS three times and treated with 0.1% Triton-X100/10% NGS for 1 h to block nonspecific binding. The sections were incubated for two days at 4 °C with the following primary antibodies: monoclonal rat anti-GFAP (1:2000; Thermo Fisher Scientific, 13-0300), monoclonal mouse anti-NeuN (1:500; Millipore, MAB377), polyclonal rabbit anti-Iba1 (1:1000; Wako, 019-19741), chicken anti-GFP antibody (1:1000, Thermo Fisher Scientific, A10262), and rabbit anti-NeuN (1:1,000; Millipore, MABN140). The sections were washed three times with PBS and then incubated for 2 h at room

545 temperature with secondary antibodies: Alexa 488- or Alexa 546-conjugated
546 goat anti-mouse/rat/rabbit or chicken IgGs (1:500; Invitrogen, A11029/Thermo
547 Fisher Scientific, A-11081/Invitrogen, A11035/Thermo Fisher Scientific,
548 A11039). After washing slices with PBS three times, they were mounted with
549 Vectashield Mounting Medium (Vector Laboratories). Fluorescence images were
550 obtained using a confocal laser microscope system (FV-1000; Olympus) or
551 Keyence fluorescence microscope (BZX-700).
552
553 **Standard quantitative RT-PCR**
554 Total RNA was isolated and purified from tissues using the RNeasy Lipid Tissue
555 Mini Kit (Qiagen) according to the manufacturer's instructions. RT-PCR
556 amplifications were performed using the One Step PrimeScript RT-PCR Kit
557 (TaKaRa Bio). RT-PCR amplifications and real-time detection were performed
558 using an Applied Biosystems 7500 Real-Time PCR System. The thermocycling
559 parameters were as follows: 5 min at 42 °C for reverse transcription, 10 s at
560 95 °C for inactivation of the RT enzyme, and 40 cycles of denaturation (5 s at 95
561 °C) and annealing/extension (34 s at 60 °C). All primer probe sets and reagents
562 were purchased from Applied Biosystems: rodent *Gapdh* (4308313), mouse *Tnf*

(Mm00443260_g1), mouse *Il1b* (Mm00434228_m1).

Dissociated cell suspensions from adult mouse brain

Three 8-week old male mice were perfused with PBS after anesthesia to eliminate serum vesicles and hippocampi were dissected to comprise one sample. Tissue dissociation was performed using the gentleMACS dissociator and the Adult Brain Dissociation Kit (Miltenyi Biotec) according to the manufacturer's protocol. Briefly, brain tissue was minced and digested with a proprietary enzyme solution on the gentleMACS dissociator adult brain program. The cells were then incubated with anti-mouse CD11b-coated microbeads (Miltenyi Biotec) for 10 min at 4 °C. The cell-bead mix was then washed to remove unbound beads. Prior to antibody labeling, nonspecific binding to the Fc receptor was blocked using the FcR Blocking Reagent (Miltenyi Biotec). Cells were suspended in PBS with 0.5% bovine serum albumin and the cell suspension was loaded onto an LS Column (Miltenyi Biotec), which was placed in the magnetic field of a QuadroMACS™ Separator (Miltenyi Biotec). The magnetically labeled CD11b positive cells were retained within the column and eluted as the positively selected cell fraction after removing the column from the

581 magnet.

582

583 **Microfluidic quantitative RT-PCR**

584 Total RNA was extracted from dissociated cells using the RNeasy Lipid Tissue
585 Mini Kit (Qiagen) and cDNA synthesis performed using the PrimeScript RT-PCR
586 Kit (Perfect Real Time) (TaKaRa Bio). For pre-amplification, up to 100 qPCR
587 assays (primer/probe sets in 20x stock concentration) were pooled and diluted to
588 a 0.2x concentration. For microfluidic qPCR, 1.25 µl of each cDNA sample was
589 pre-amplified using 1 µl of TaqMan pre-amplification master mix (PN 100-5580,
590 Fluidigm), 1.25 µl of the primer pool, and 1.5 µl of water. Pre-amplification was
591 performed using a 2 min 95 °C denaturation step and 14 cycles of 15 s at 95 °C
592 and 4 min at 60 °C. Microfluidic quantitative RT-PCR reactions were performed
593 using the 96x96 chips and included 2–3 technical replicates for each
594 combination of sample and assay. For sample mixtures, 2.7 µl pre-amplification
595 product was combined with 0.3 µl of 20x GE Sample Loading Reagent
596 (85000746, Fluidigm) and 3 µl of 2x PCR master mix (4324020, Thermo Fisher
597 Scientific), of which 5 µl of was loaded into sample wells. For assay mixtures,
598 equal volumes of TaqMan assay and 2x Assay Loading Reagent (PN85000736,

599 Fluidigm) were combined, and 5 µl of the resulting mixture was loaded into
600 multiple assay wells. RT-PCR amplifications and real-time detection were
601 performed using the BioMarkHD Real-Time PCR System (Fluidigm). Data from
602 Fluidigm runs were manually checked for reaction quality prior to analysis, and
603 Ct values for each gene target were normalized to Ct values for housekeeping
604 genes. All primer probe sets and reagents were purchased from Integrated DNA
605 Technologies: rodent *Gapdh* (Mm.PT.39a.1), mouse *Tnf* (Mm.PT.58.12575861),
606 mouse *Il1b* (Mm.PT.58.41616450), mouse *Cx3cr1* (Mm.PT.58.17555544),
607 mouse *CD45* (Mm.PT.58.7583849), mouse *CD11b* (Mm.PT.58.14195622),
608 mouse *CD68* (Mm.PT.58.32698807), mouse *CD206* (Mm.PT.58.42560062),
609 mouse *Il6* (Mm.PT.58.10005566), mouse *Ifng* (Mm.PT.58.41769240), mouse *Il4*
610 (Mm.PT.58.32703659), mouse *Il10* (Mm.PT.58.13531087), and mouse *Tgfb*
611 (Mm.PT.58.11254750).

612

613 **Preparation of brain slices and Ca^{2+} imaging**

614 The methods used have been described previously [56,70]. Briefly, 8-week-old
615 male mice were anesthetized with pentobarbital (100 mg kg^{-1}, i.p.). Cold cutting
616 ACSF, composed of 92 mM NaCl, 2.5 mM KCl, 1.2 mM NaH_2PO_4, 30 mM

617 $NaHCO_3$, 20 mM HEPES, 25 mM D-glucose, 5 mM sodium ascorbate, 2 mM
618 thiourea, 3 mM sodium pyruvate, 10 mM $MgCl_2$, and 0.5 mM $CaCl_2$ saturated
619 with 95% O_2–5% CO_2, was perfused transcardially. Coronal slices of the
620 hippocampus (300 µm) were cut using a vibrating microtome (Pro7, Dosaka) in
621 cutting ACSF. Slices were incubated at 34 °C for 10 min in recovery ACSF,
622 composed of 93 mM N-methyl-D-glucamine, 93 mM HCl, 2.5 mM KCl, 1.2 mM
623 NaH_2PO_4, 30 mM $NaHCO_3$, 20 mM HEPES, 25 mM D-glucose, 5 mM sodium
624 ascorbate, 2 mM thiourea, 3 mM sodium pyruvate, 10 mM $MgCl_2$, and 0.5 mM
625 $CaCl_2$ saturated with 95% O_2–5% CO_2, and subsequently stored in ACSF
626 comprising 124 mM NaCl, 2.5 mM KCl, 1.2 mM NaH_2PO_4, 24 mM $NaHCO_3$, 5
627 mM HEPES, 12.5 mM D-glucose, 5 mM sodium ascorbate, 2 mM thiourea, 3 mM
628 sodium pyruvate, 2 mM $MgCl_2$, and 2 mM $CaCl_2$ saturated with 95% O_2 and 5%
629 CO_2 at room temperature. After 1 h of recovery, slices were submerged in ACSF
630 at approximately 32 °C. Slices were imaged using an Olympus Fluoview
631 FVMPE-RS two-photon laser scanning microscope equipped with a Maitai HP
632 DS-OL laser (Spectra-Physics). We used a 920 nm laser and 510 nm high-pass
633 emission filter. Astrocytes were selected from the CA1 stratum radiatum region
634 and were typically 30–50 µm from the slice surface. Images were gathered using

635 a 25× water immersion lens with a numerical aperture of 1.05.

636 For Fluo-4AM measurements, we dropped 2.5 µl Fluo-4AM (2 mM) onto the
637 hippocampal slices followed by incubation in ACSF for 60 min, then transferred
638 the slices to dye-free ACSF for at least 30 min prior to experimentation. The final
639 concentration of Fluo4-AM was 5 µM with 0.02% Pluronic F–127. Astrocytes
640 were selected from the CA1 stratum radiatum region and were typically 30–50
641 µm from the slice surface. TTX (1 µM), 2-APB (100 µM), and CPA (20 µM) were
642 solubilized in ACSF. Baseline astrocytic activity was recorded prior to drug
643 application. Subsequently, drugs were applied onto the slice for 10 min and
644 astrocytic activity was recorded for 10 min.

645

646 **Image analysis**

647 Images were acquired using inverted confocal laser-scanning systems (Olympus
648 FV-1000) at 40× magnification with a 1.30 numerical aperture objective lens.
649 Information regarding z-stack images is described in the figure legends.
650 Astrocytes were selected from the CA1 stratum radiatum region and imaged
651 based on GFAP immunostaining. Microglia were imaged based on Iba1
652 immunostaining at the CA1 stratum radiatum region. Subsequent images were

processed and quantified using ImageJ (US National Institutes of Health; NIH). For the quantitative analysis of the area containing Iba1 positive microglia, we randomly chose three fields per mouse. Images were converted to gray scale and the quantification threshold was set constantly for all specimens within each experimental group. The percentage of Iba1-positive area was calculated by dividing the area of Iba1-positive region by the total area of the region of interest. For the quantitative analysis of GFAP positive cell size, we randomly chose one field per mouse. Images were converted to gray scale and the quantification threshold was set constantly for all specimens within each experimental group. To quantify the GFAP positive cell size, particles were analyzed based on GFAP immunoreactivity and we chose the three largest GFAP positive cells per field.

The methods used for Ca^{2+} imaging data analysis have been described previously [56,70]. Briefly, imaging data were analyzed using ImageJ. We selected regions of interest from somatic regions of astrocytes by visual examination of the time lapse image. Using these regions of interest, raw fluorescence intensity values (F) were taken from the original videos and converted to delta F/F (dF/F) in Originlab (Origin Lab Corp.). We analyzed Ca^{2+} signals when their dF/F values were greater than 0.2. We analyzed Ca^{2+} signals

and their amplitude (dF/F) and duration (full width at half maximum) using the Originlab “peak analysis” function.

Statistical analysis

All statistical analyses were performed using SPSS version 19.0 (SPSS Inc.) software. Data are presented as the means ± SEM. Most data were analyzed using one-way ANOVA followed by Dunnett’s multiple post hoc test for comparing more than three samples, and two-sample unpaired *t*-tests. *P* values <0.05 were considered as statistically significant.

Acknowledgements

We thank Dr. K. Takanashi, Mr. R. Komatsu, Mrs. Y. Fukasawa, Mrs. M. Tachibana, Mrs. Y. Koseki, and Mrs. Y. Hoshino (Univ. Yamanashi) for technical assistance, and all members of the Koizumi Laboratory for critical discussion.

687 **References**

688 1. Engel J Jr. Mesial temporal lobe epilepsy: what have we learned?
689 Neuroscientist. 2001;7(4): 340-52.

690 2. Herman ST. Epilepsy after brain insult: targeting epileptogenesis. Neurology.
691 2002;59(9 Suppl 5): S21-26.

692 3. French JA, Williamson PD, Thadani VM, Darcey TM, Mattson RH, Spencer
693 SS, et al. Characteristics of medial temporal lobe epilepsy: I. Results of history
694 and physical examination. Ann Neurol. 1993;34(6): 774- 80.

695 4. Rakhade SN, Jensen FE. Epileptogenesis in the immature brain: emerging
696 mechanisms. Nat Rev Neurol. 2009;5(7): 380-391.

697 5. Binder DK, Steinhauser C. Functional changes in astroglial cells in epilepsy.
698 Glia. 2006;54(5): 358-368.

699 6. Seifert G, Steinhauser C. Neuron-astrocyte signaling and epilepsy. Exp
700 Neurol. 2013;244: 4-10.

701 7. Shapiro LA, Wang L, Ribak CE. Rapid astrocyte and microglial activation
702 following pilocarpine-induced seizures in rats. Epilepsia. 2008;49 Suppl 2:
703 33-41.

704 8. Benson MJ, Manzanero S, Borges K. Complex alterations in microglial M1/M2

markers during the development of epilepsy in two mouse models. Epilepsia. 2015;56(6): 895-905.

9. Vezzani A, French J, Bartfai T, Baram TZ. The role of inflammation in epilepsy. Nat Rev Neurol. 2011;7(1): 31-40.

10. Boer K, Spliet WG, van Rijen PC, Redeker S, Troost D, Aronica E. Evidence of activated microglia in focal cortical dysplasia. J Neuroimmunol. 2006;173(1-2): 188-195.

11. Vezzani A, Moneta D, Richichi C, Aliprandi M, Burrows SJ, Ravizza T, et al. Functional role of inflammatory cytokines and antiinflammatory molecules in seizures and epileptogenesis. Epilepsia. 2002;43 Suppl 5: 30-35.

12. Cendes F, Sakamoto AC, Spreafico R, Bingaman W, Becker AJ. Epilepsies associated with hippocampal sclerosis. Acta Neuropathol. 2014;128(1): 21-37.

13. Morizawa YM, Hirayama Y, Ohno N, Shibata S, Shigetomi E, Sui Y, et al. Author Correction: Reactive astrocytes function as phagocytes after brain ischemia via ABCA1-mediated pathway. Nat Commun. 2017;8(1): 1598.

14. Haj-Yasein NN, Jensen V, Vindedal GF, Gundersen GA, Klungland A, Ottersen OP, et al. Evidence that compromised K+ spatial buffering contributes to the epileptogenic effect of mutations in the human Kir4.1 gene (KCNJ10).

723 Glia. 2011;59(11): 1635-1642.

724 15. Tanaka K, Watase K, Manabe T, Yamada K, Watanabe M, Takahashi K, et
725 al. Epilepsy and exacerbation of brain injury in mice lacking the glutamate
726 transporter GLT-1. Science. 1997;276(5319): 1699-1702.

727 16. Bezzi P, Gundersen V, Galbete JL, Seifert G, Steinhauser C, Pilati E, et al.
728 Astrocytes contain a vesicular compartment that is competent for regulated
729 exocytosis of glutamate. Nat Neurosci. 2004;7(6): 613-620.

730 17. Devinsky O, Vezzani A, Najjar S, De Lanerolle NC, Rogawski MA. Glia and
731 epilepsy: excitability and inflammation. Trends Neurosci. 2013;36(3): 174-184.

732 18. Charles AC, Merrill JE, Dirksen ER, Sanderson MJ. Intercellular signaling in
733 glial cells: calcium waves and oscillations in response to mechanical stimulation
734 and glutamate. Neuron. 1991;6(6): 983-992.

735 19. Cornell-Bell AH, Finkbeiner SM, Cooper MS, Smith SJ. Glutamate induces
736 calcium waves in cultured astrocytes: long-range glial signaling. Science.
737 1990;247(4941): 470-473.

738 20. Allen NJ, Eroglu C. Cell biology of astrocyte-synapse interactions. Neuron.
739 2017;96(3): 697-708.

740 21. Araque A, Carmignoto G, Haydon PG, Oliet SH, Robitaille R, Volterra A.

741 Gliotransmitters travel in time and space. Neuron. 2014;81(4): 728-739.

742 22. Kim SK, Hayashi H, Ishikawa T, Shibata K, Shigetomi E, Shinozaki Y, et al.
743 Cortical astrocytes rewire somatosensory cortical circuits for peripheral
744 neuropathic pain. J Clin Invest. 2016;126(5): 1983-1997.

745 23. Halassa MM, Fellin T, Haydon PG. The tripartite synapse: roles for
746 gliotransmission in health and disease. Trends Mol Medi. 2007;13(2): 54-63.

747 24. Ding S, Fellin T, Zhu Y, Lee SY, Auberson YP, Meaney DF, et al. Enhanced
748 astrocytic Ca2+ signals contribute to neuronal excitotoxicity after status
749 epilepticus. J Neurosci. 2007;27(40): 10674-10684.

750 25. Tian GF, Azmi H, Takano T, Xu Q, Peng W, Lin J, et al. An astrocytic basis of
751 epilepsy. Nat Med. 2005;11(9): 973-981.

752 26. Curia G, Longo D, Biagini G, Jones RS, Avoli M. The pilocarpine model of
753 temporal lobe epilepsy. J Neurosci Methods. 2008;172(2): 143-157.

754 27. Levesque M, Avoli M, Bernard C. Animal models of temporal lobe epilepsy
755 following systemic chemoconvulsant administration. J Neurosc Methods.
756 2016;260: 45-52.

757 28. Clasadonte J, Dong J, Hines DJ, Haydon PG. Astrocyte control of synaptic
758 NMDA receptors contributes to the progressive development of temporal lobe

759 epilepsy. Proc Natl Acad Sci U S A. 2013;110(43): 17540-17545.

760 29. Groticke I, Hoffmann K, Loscher W. Behavioral alterations in a mouse model
761 of temporal lobe epilepsy induced by intrahippocampal injection of kainate. Exp
762 Neurol. 2008;213(1): 71-83.

763 30. Mori T, Tanaka K, Buffo A, Wurst W, Kuhn R, Gotz M. Inducible gene
764 deletion in astroglia and radial glia--a valuable tool for functional and lineage
765 analysis. Glia. 2006;54(1): 21-34.

766 31. Zariwala HA, Borghuis BG, Hoogland TM, Madisen L, Tian L, De Zeeuw CI,
767 et al. A Cre-dependent GCaMP3 reporter mouse for neuronal imaging in vivo. J
768 Neurosci. 2012;32(9): 3131-3141.

769 32. Futatsugi A, Nakamura T, Yamada MK, Ebisui E, Nakamura K, Uchida K, et
770 al. IP3 receptor types 2 and 3 mediate exocrine secretion underlying energy
771 metabolism. Science. 2005;309(5744): 2232-2234.

772 33. Abraham J, Fox PD, Condello C, Bartolini A, Koh S. Minocycline attenuates
773 microglia activation and blocks the long-term epileptogenic effects of early-life
774 seizures. Neurobiol Dis. 2012;46(2): 425-430.

775 34. Hirayama Y, Ikeda-Matsuo Y, Notomi S, Enaida H, Kinouchi H, Koizumi S.
776 Astrocyte-mediated ischemic tolerance. J Neurosci. 2015;35(9): 3794-3805.

777 35. Matsuda T, Murao N, Katano Y, Juliandi B, Kohyama J, Akira S, et al. TLR9
778 signalling in microglia attenuates seizure-induced aberrant neurogenesis in the
779 adult hippocampus. Nat Commun. 2015;6: 6514.
780 36. Dagher NN, Najafi AR, Kayala KM, Elmore MR, White TE, Medeiros R, et al.
781 Colony-stimulating factor 1 receptor inhibition prevents microglial plaque
782 association and improves cognition in 3xTg-AD mice. J Neuroinflamm. 2015;12:
783 139.
784 37. Shinozaki Y, Shibata K, Yoshida K, Shigetomi E, Gachet C, Ikenaka K, et al.
785 Transformation of astrocytes to a neuroprotective phenotype by microglia via
786 P2Y1 receptor downregulation. Cell Rep. 2017;19(6): 1151-1164.
787 38. Valdearcos M, Robblee MM, Benjamin DI, Nomura DK, Xu AW, Koliwad SK.
788 Microglia dictate the impact of saturated fat consumption on hypothalamic
789 inflammation and neuronal function. Cell Rep. 2014;9(6): 2124-2138.
790 39. Avignone E, Ulmann L, Levavasseur F, Rassendren F, Audinat E. Status
791 epilepticus induces a particular microglial activation state characterized by
792 enhanced purinergic signaling. J Neurosci. 2008;28(37): 9133-9144.
793 40. Koizumi S, Shigemoto-Mogami Y, Nasu-Tada K, Shinozaki Y, Ohsawa K,
794 Tsuda M, et al. UDP acting at P2Y6 receptors is a mediator of microglial

phagocytosis. Nature. 2007;446(7139): 1091-1095.

41. Pekny M, Nilsson M. Astrocyte activation and reactive gliosis. Glia. 2005;50(4): 427-434.

42. Sofroniew MV, Vinters HV. Astrocytes: biology and pathology. Acta Neuropathol. 2010;119(1): 7-35.

43. Eyo UB, Murugan M, Wu LJ. Microglia-neuron communication in epilepsy. Glia. 2017;65(1): 5-18.

44. Stellwagen D, Beattie EC, Seo JY, Malenka RC. Differential regulation of AMPA receptor and GABA receptor trafficking by tumor necrosis factor-alpha. J Neurosci. 2005;25(12): 3219-3228.

45. Campbell IL, Abraham CR, Masliah E, Kemper P, Inglis JD, Oldstone MB, et al. Neurologic disease induced in transgenic mice by cerebral overexpression of interleukin 6. Proc Natl Acad Sci U S A. 1993;90(21): 10061-10065.

46. Samland H, Huitron-Resendiz S, Masliah E, Criado J, Henriksen SJ, Campbell IL. Profound increase in sensitivity to glutamatergic- but not cholinergic agonist-induced seizures in transgenic mice with astrocyte production of IL-6. J Neurosci Res. 2003;73(2): 176-187.

47. Coulter DA, Steinhauser C. Role of astrocytes in epilepsy. Cold Spring Harb

813 Perspect Med. 2015;5(3): a022434.

814 48. Seifert G, Carmignoto G, Steinhauser C. Astrocyte dysfunction in epilepsy.

815 Brain Res Rev. 2010;63(1-2): 212-221.

816 49. Steinhauser C, Grunnet M, Carmignoto G. Crucial role of astrocytes in

817 temporal lobe epilepsy. Neuroscience. 2016;323: 157-169.

818 50. Alvarez-Ferradas C, Morales JC, Wellmann M, Nualart F, Roncagliolo M,

819 Fuenzalida M, et al. Enhanced astroglial Ca2+ signaling increases excitatory

820 synaptic strength in the epileptic brain. Glia. 2015;63(9): 1507-1521.

821 51. Gomez-Gonzalo M, Losi G, Chiavegato A, Zonta M, Cammarota M, Brondi

822 M, et al. An excitatory loop with astrocytes contributes to drive neurons to

823 seizure threshold. PLoS Biol. 2010;8(4): e1000352.

824 52. Bazargani N, Attwell D. Astrocyte calcium signaling: the third wave. Nat

825 Neurosci. 2016;19(2): 182-189.

826 53. Haydon PG. GLIA: listening and talking to the synapse. Nat Rev Neurosci.

827 2001;2(3): 185-193.

828 54. Weissberg I, Wood L, Kamintsky L, Vazquez O, Milikovsky DZ, Alexander A,

829 et al. Albumin induces excitatory synaptogenesis through astrocytic

830 TGF-beta/ALK5 signaling in a model of acquired epilepsy following blood-brain

barrier dysfunction. Neurobiol Dis. 2015;78: 115-125.

55. Berridge MJ, Bootman MD, Roderick HL. Calcium signalling: dynamics, homeostasis and remodelling. Nat Rev Mol Cell Biol. 2003;4(7): 517-529.

56. Saito K, Shigetomi E, Yasuda R, Sato R, Nakano M, Tashiro K, et al. Aberrant astrocyte Ca(2+) signals "AxCa signals" exacerbate pathological alterations in an Alexander disease model. Glia. 2018;66(5): 1053-1067.

57. Bedner P, Dupper A, Huttmann K, Muller J, Herde MK, Dublin P, et al. Astrocyte uncoupling as a cause of human temporal lobe epilepsy. Brain. 2015;138(Pt 5): 1208-1222.

58. Bordey A, Lyons SA, Hablitz JJ, Sontheimer H. Electrophysiological characteristics of reactive astrocytes in experimental cortical dysplasia. J Neurophysiol. 2001;85(4): 1719-1731.

59. Bordey A, Sontheimer H. Properties of human glial cells associated with epileptic seizure foci. Epilepsy Res. 1998;32(1-2): 286-303.

60. Steinhauser C, Seifert G, Bedner P. Astrocyte dysfunction in temporal lobe epilepsy: K+ channels and gap junction coupling. Glia. 2012;60(8): 1192-1202.

61. Liddelow SA, Guttenplan KA, Clarke LE, Bennett FC, Bohlen CJ, Schirmer L, et al. Neurotoxic reactive astrocytes are induced by activated microglia. Nature.

2017;541(7638): 481-487.

62. Dheen ST, Kaur C, Ling EA. Microglial activation and its implications in the brain diseases. Curr Med Chem. 2007;14(11): 1189-1197.

63. Kingwell K. Neurodegenerative disease: Microglia in early disease stages. Nat Rev Neurol. 2012;8(9): 475.

64. Shinozaki Y, Nomura M, Iwatsuki K, Moriyama Y, Gachet C, Koizumi S. Microglia trigger astrocyte-mediated neuroprotection via purinergic gliotransmission. Sci Repo. 2014;4: 4329.

65. Riazi K, Galic MA, Kuzmiski JB, Ho W, Sharkey KA, Pittman QJ. Microglial activation and TNFalpha production mediate altered CNS excitability following peripheral inflammation. Proc Nl Acad Sci U S A. 2008;105(44): 17151-17156.

66. Vezzani A, Conti M, De Luigi A, Ravizza T, Moneta D, Marchesi F, et al. Interleukin-1beta immunoreactivity and microglia are enhanced in the rat hippocampus by focal kainate application: functional evidence for enhancement of electrographic seizures. J Neurosci. 1999;19(12): 5054-5065.

67. John GR, Lee SC, Brosnan CF. Cytokines: powerful regulators of glial cell activation. Neuroscientist. 2003;9(1): 10-22.

68. Sofroniew MV. Molecular dissection of reactive astrogliosis and glial scar

867 formation. Trends Neurosc. 2009;32(12): 638-647.

868 69. Imura Y, Morizawa Y, Komatsu R, Shibata K, Shinozaki Y, Kasai H, et al.

869 Microglia release ATP by exocytosis. Glia. 2013;61(8): 1320-1330.

870 70. Shigetomi E, Hirayama YJ, Ikenaka K, Tanaka KF, Koizumi S. Role of

871 purinergic receptor P2Y1 in spatiotemporal Ca(2+) dynamics in astrocytes. J

872 Neurosci. 2018;38(6): 1383-1395.

873

874 **Supporting Information**

875 **S1 Fig** Initial microglial activation is observed after SE in IP3R2KO mice.

876 **S2 Fig** Immunohistochemical analysis of GCaMP expression in the

877 hippocampus in Glast-CreERT2::Flx-GCaMP3 mice.

878 **S1 Table** Cell-specific markers in GCaMP3-expressing cells in the hippocampus

879 of Glast-CreERT2::Flx-GCaMP3 mice (tamoxifen i.p. at P7).

880 **S1 Movie** Ca^{2+} dynamics of astrocytes in the CA1 stratum radiatum region in

881 Glast-CreERT2::flx-GCaMP3 control mice and approximately 4 weeks after SE

882 with or without minocycline treatment.

883 **S2 Movie** Ca^{2+} dynamics of astrocytes approximately 4 weeks after SE in the

884 CA1 stratum radiatum region in Glast-CreERT2::flx-GCaMP3 mice before and

885 after TTX application.

886 **S3 Movie** Ca^{2+} dynamics of astrocytes approximately 4 weeks after SE in the
887 CA1 stratum radiatum region in Glast-CreERT2::flx-GCaMP3 mice before and
888 after CPA application.

889 **S4 Movie** Ca^{2+} dynamics of astrocytes approximately 4 weeks after SE in the
890 CA1 stratum radiatum region in Glast-CreERT2::flx-GCaMP3 mice before and
891 after 2-APB application.

892 **S5 Movie** Astrocytic Ca^{2+} dynamics as revealed by Fluo4 in the CA1 stratum
893 radiatum region in WT control, WT after SE, and IP_3R2KO mice after SE.

894 **S6 Movie** Ca^{2+} dynamics of astrocytes approximately 4 weeks after SE in the
895 CA1 stratum radiatum region in Glast-CreERT2::flx-GCaMP3 mice.

896 **S7 Movie** Ca^{2+} dynamics of astrocytes approximately 4 weeks after SE in the
897 CA1 stratum radiatum region in Glast-CreERT2::flx-GCaMP3 mice with or
898 without PLX5622 treatment.

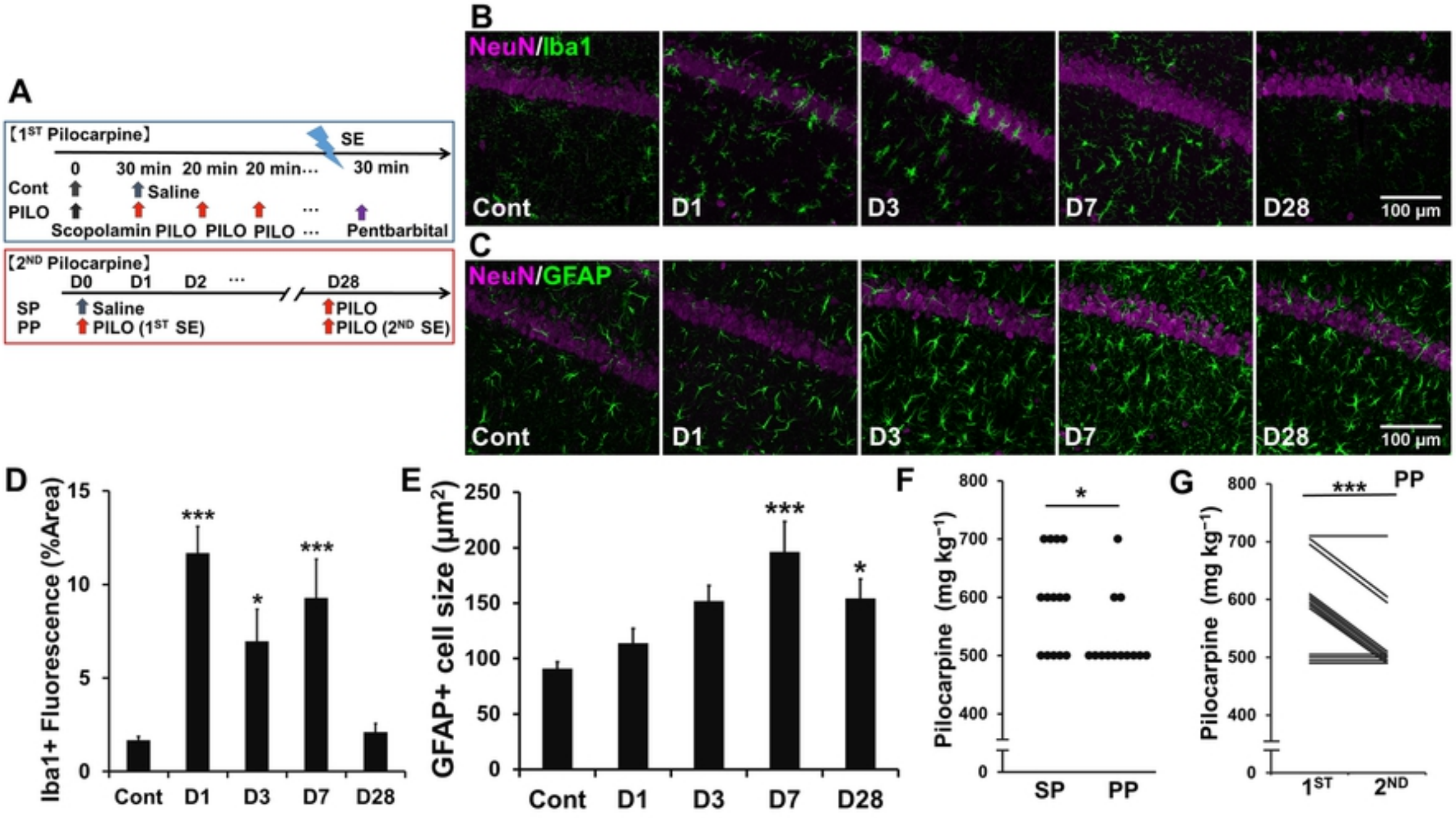
A
【1ST Pilocarpine】
SE
0
30 min
20 min
20 min
30 min
Cont
Saline
PILO
Scopolamin
PILO
PILO
PILO
Pentbarbital
【2ND Pilocarpine】
D0
D1
D2
D28
SP
Saline
PILO
PP
PILO (1ST SE)
PILO (2ND SE)
B
NeuN/Iba1
Cont
D1
D3
D7
D28
100 μm
C
NeuN/GFAP
Cont
D1
D3
D7
D28
100 μm
D
Iba1+ Fluorescence (%Area)
Cont
D1
D3
D7
D28
E
GFAP+ cell size (μm2)
Cont
D1
D3
D7
D28
F
Pilocarpine (mg kg−1)
SP
PP
G
PP
Pilocarpine (mg kg−1)
1ST
2ND

Figure 1

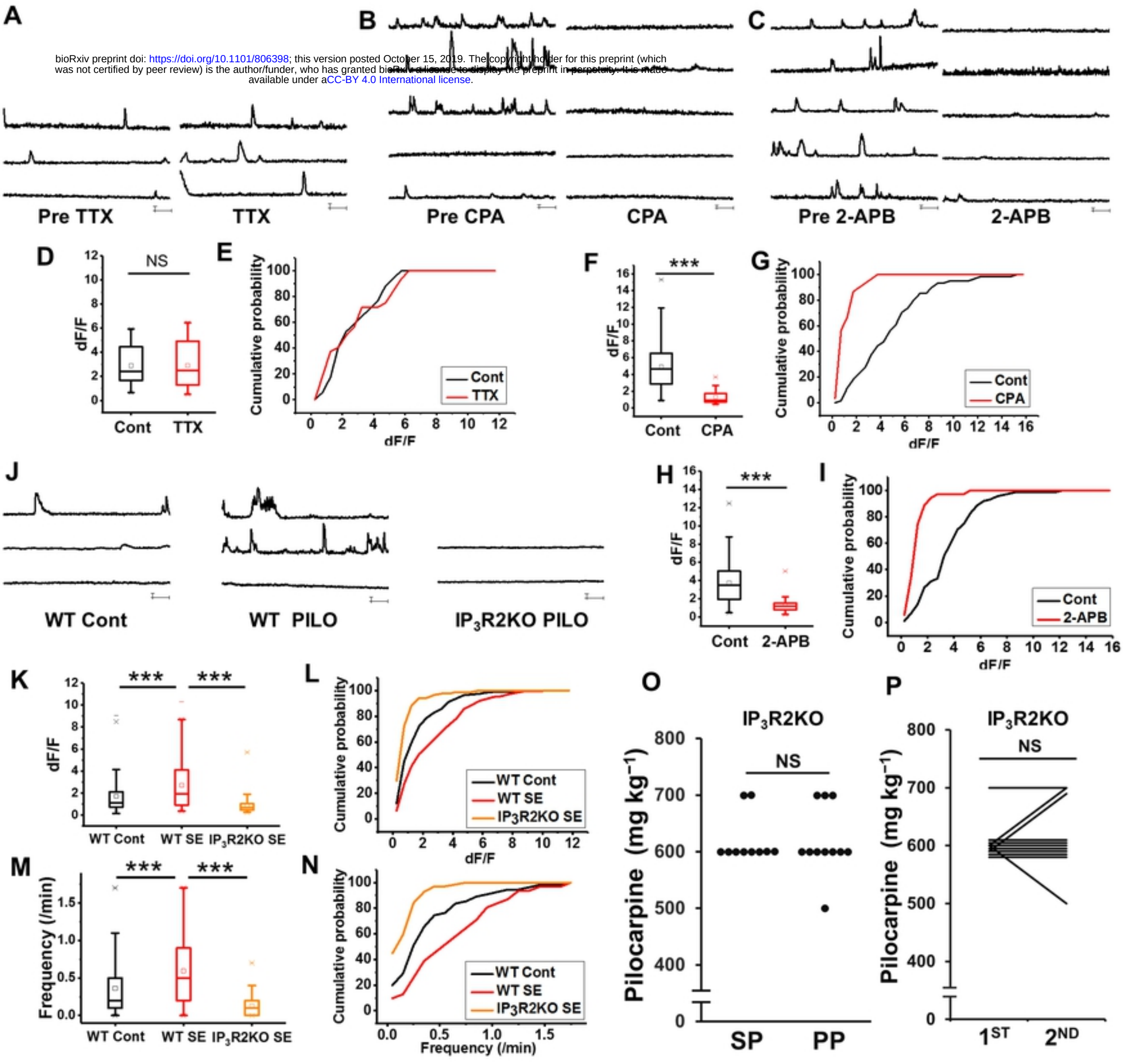

Figure 2

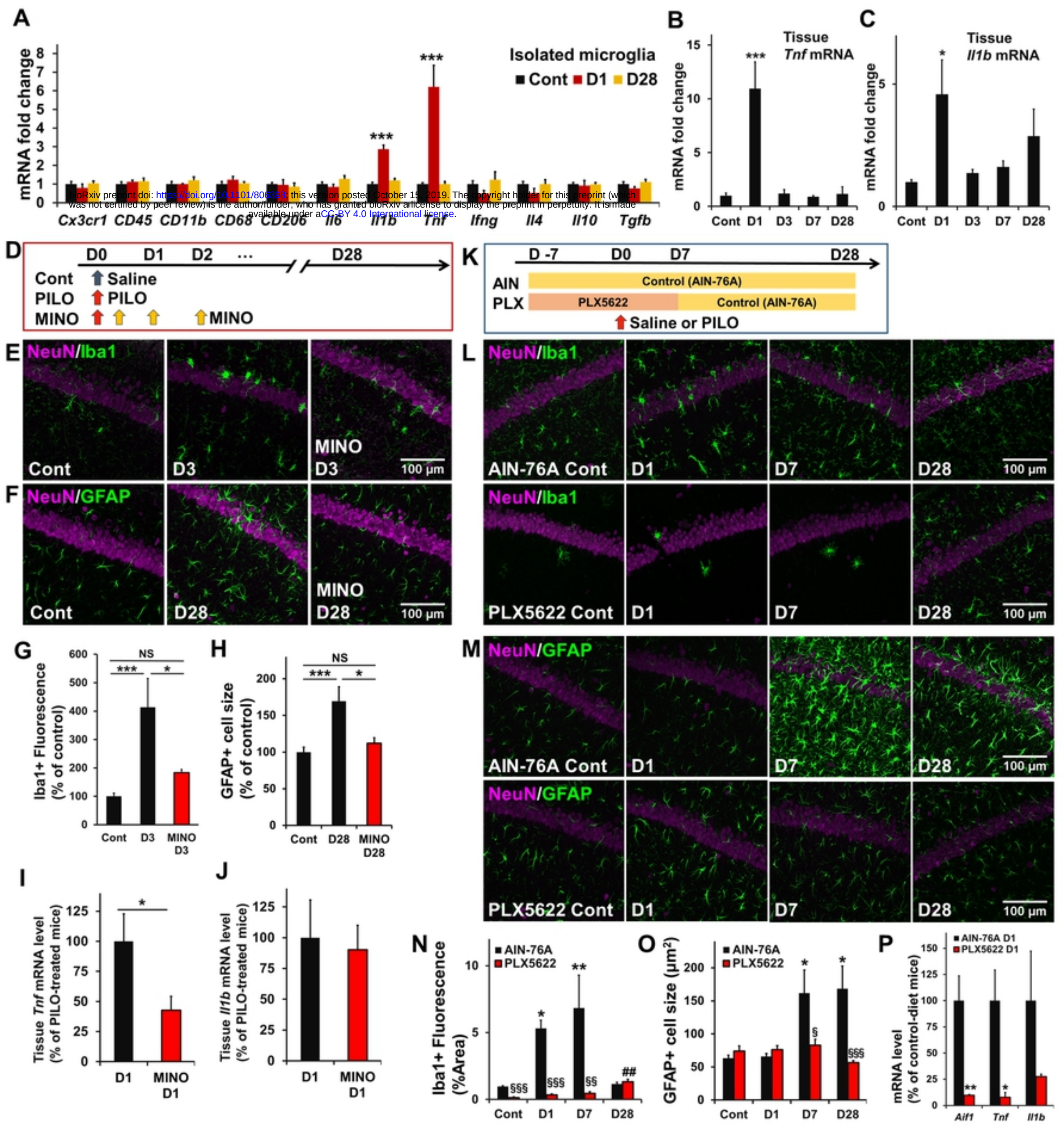

Figure 3

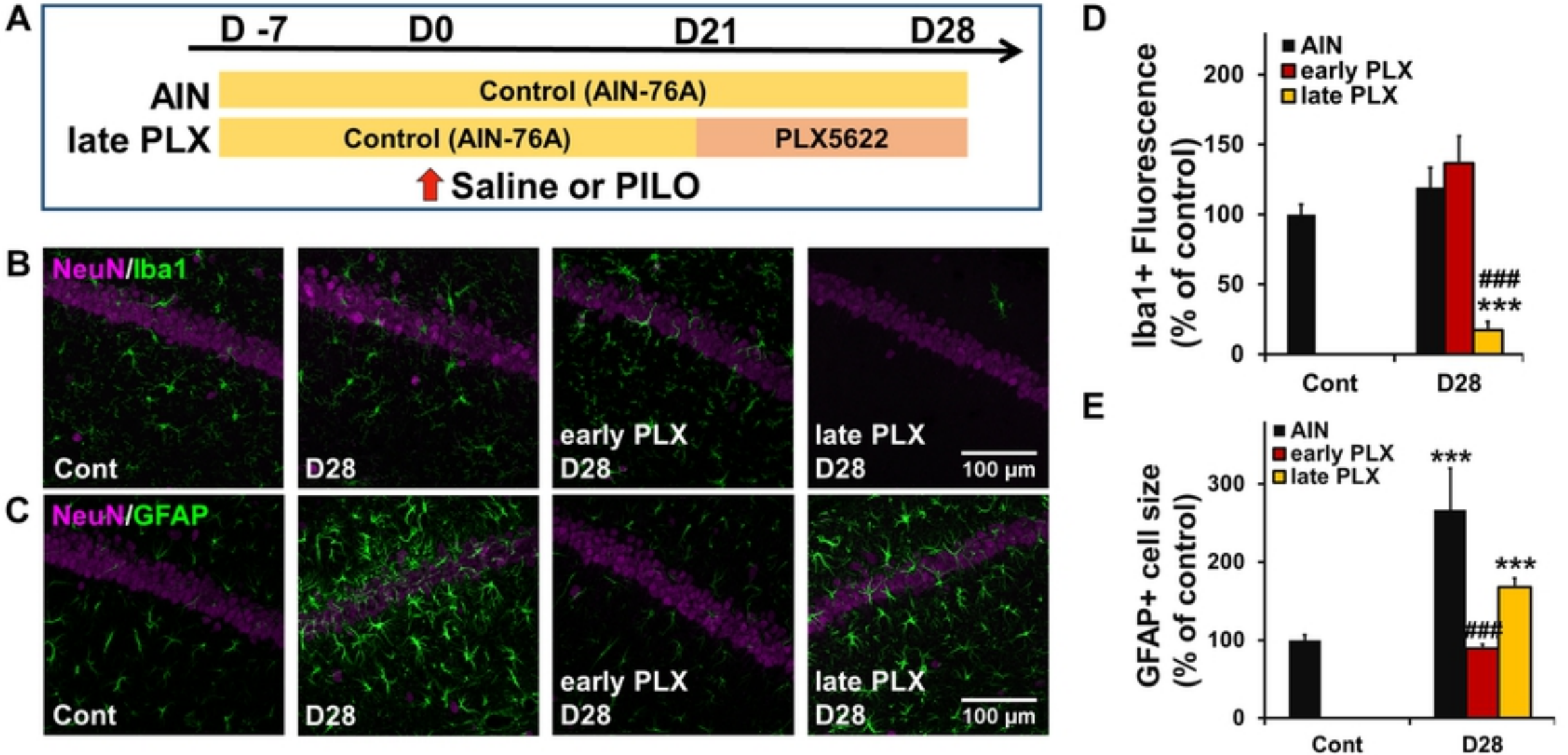
A
D -7
D0
D21
D28
AIN
Control (AIN-76A)
late PLX
Control (AIN-76A)
PLX5622
Saline or PILO
B
NeuN/Iba1
Cont
D28
early PLX
D28
late PLX
D28
100 µm
C
NeuN/GFAP
Cont
D28
early PLX
D28
late PLX
D28
100 µm
D
AIN
early PLX
late PLX
Iba1+ Fluorescence
(% of control)
200
150
100
50
0
###
***
Cont
D28
E
AIN
early PLX
late PLX
GFAP+ cell size
(% of control)
300
200
100
0
***
###
***
Cont
D28

Figure 4

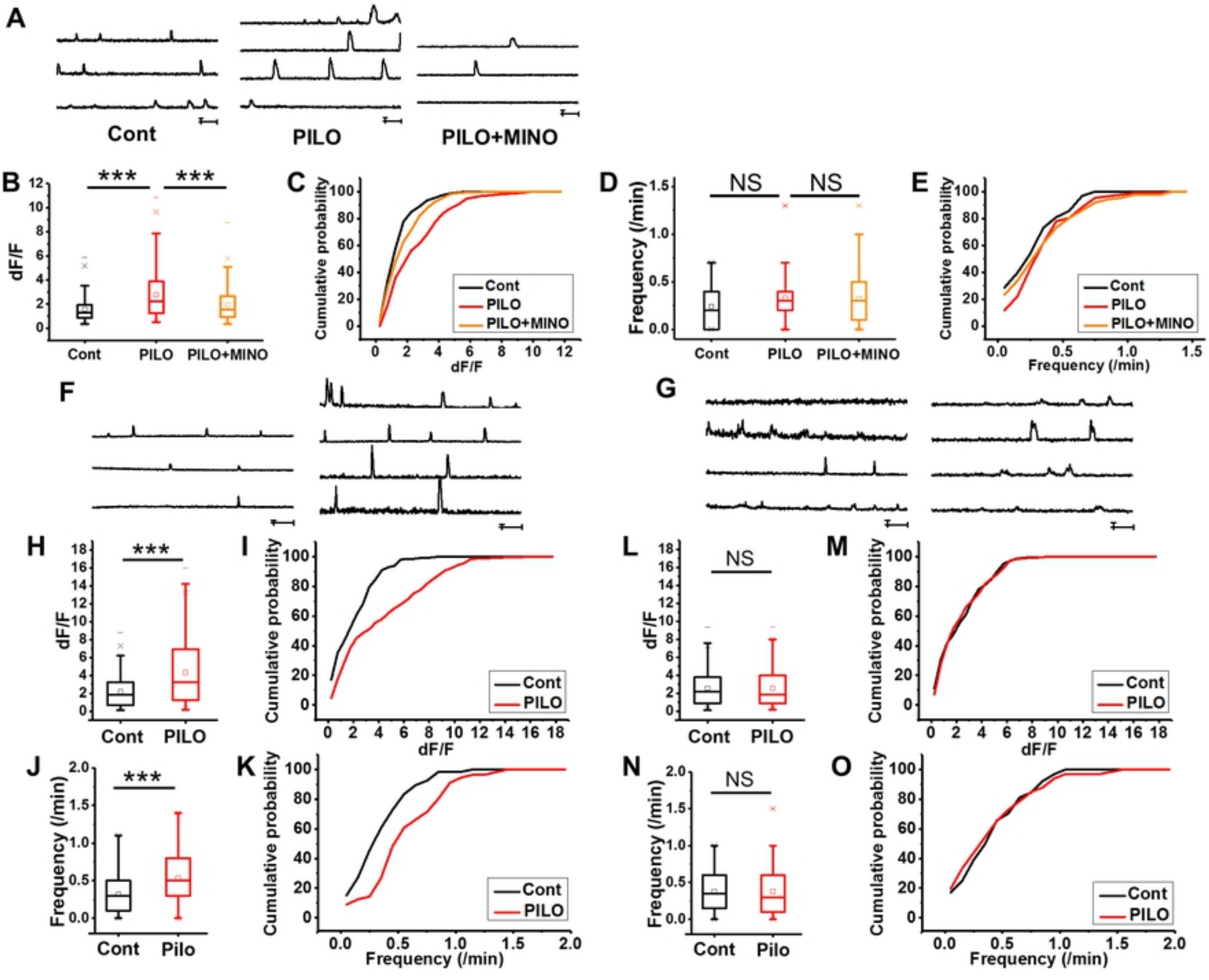
A
Cont
PILO
PILO+MINO
B
***
***
dF/F
Cont
PILO
PILO+MINO
C
Cumulative probability
dF/F
Cont
PILO
PILO+MINO
D
NS
NS
Frequency (/min)
Cont
PILO
PILO+MINO
E
Cumulative probability
Frequency (/min)
Cont
PILO
PILO+MINO
F
G
H
***
dF/F
Cont
PILO
I
Cumulative probability
dF/F
Cont
PILO
L
NS
dF/F
Cont
PILO
M
Cumulative probability
dF/F
Cont
PILO
J
***
Frequency (/min)
Cont
Pilo
K
Cumulative probability
Frequency (/min)
Cont
PILO
N
NS
Frequency (/min)
Cont
Pilo
O
Cumulative probability
Frequency (/min)
Cont
PILO

Figure 5

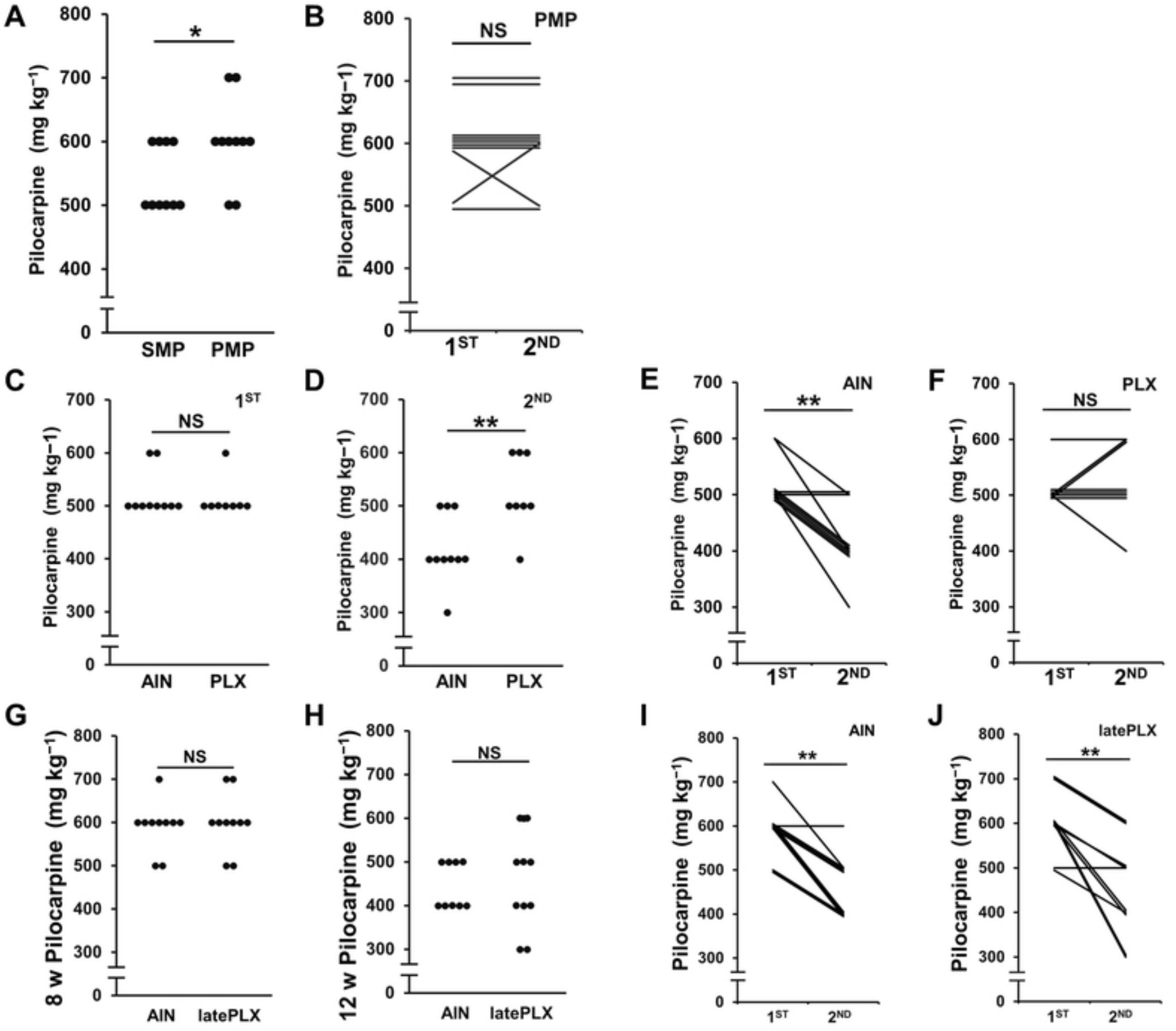
A
B
C
D
E
F
G
H
I
J
Pilocarpine (mg kg−1)
8 w Pilocarpine (mg kg−1)
12 w Pilocarpine (mg kg−1)
800
700
600
500
400
300
0
*
NS
**
SMP
PMP
1ST
2ND
AIN
PLX
latePLX

Figure 6